

Nanodust in the Interstellar Medium in Comparison to the Solar System

Aigen Li and Ingrid Mann

Abstract Nanodust, which undergoes stochastic heating by single starlight photons and dominates the near- and mid-infrared emission in the interstellar medium, ranges from angstrom-sized large molecules containing tens to thousands of atoms to grains of a couple of tens of nanometers. The presence of nanodust in astrophysical environments has been revealed by a variety of phenomena: the optical luminescence, the near- and mid-infrared continuum emission and spectral bands, the Galactic foreground microwave emission, and the ultraviolet extinction. These phenomena are ubiquitously seen in the interstellar medium of the Milky Way and beyond.

Nanometre-sized grains have also been identified as presolar in primitive meteorites based on their isotopically anomalous composition. Considering the very processes that reveal the presence of nanodust in the ISM for the nanodust in the solar system shows that observing solar system nanodust through these processes is less likely.

1 Introduction: The Interstellar Medium and Nanodust

The stars in our Galaxy, the Milky Way, are far apart and, for instance the nearest star, Proxima Centauri, is at distance roughly 1.3 parsec (pc¹) from the Sun. The space between stars contains gaseous ions, atoms, molecules and solid dust grains:

¹With 1 pc = 3.086×10^{16} m this is $\sim 2.67 \times 10^5$ AU, where 1 AU = 1.496×10^{11} m is the average distance between Sun and Earth.

A. Li (✉)

Department of Physics and Astronomy, University of Missouri, Columbia, MO 65211, USA
e-mail: lia@missouri.edu

I. Mann

Belgium Institute for Space Aeronomie, 3 Avenue Circulaire, 1180 Brussels, Belgium
e-mail: ingrid.mann@aeronomie.be

the interstellar medium (ISM). With a mean number density of ~ 1 H-atom/cm³ it is more empty than the best vacuum (which has a density of $\sim 10^3$ molecules/cm³) that can be created on Earth. The gas and dust of the ISM contain $\sim 10\%$ of the total mass of the visible matter in the present-day Milky Way.² The bulk of the heavy elements, including most of the interstellar silicon, magnesium, iron and a large fraction of the interstellar carbon, are depleted from the gas phase and form submicron-sized grains, which make up $\sim 1\%$ of the total mass of the ISM. In a spiral galaxy like the Milky Way, most of the interstellar dust and gas are concentrated in its spiral arms and a relatively thin gaseous disk of a thickness of a few hundred pc.

The ISM plays a crucial role in galaxy evolution: New stars form out of dusty molecular clouds which present a dense phase of the ISM while stars in late stage of evolution return gas and newly formed dust to the ISM (either through stellar winds or supernova explosions). The astrophysics of the ISM, from the thermodynamics and chemistry of the gas to the dynamics of star formation, is strongly influenced by the presence of the dust. Dust particles within the ISM are subject to various processes of destruction (e.g., sublimation, collisional fragmentation, sputtering) and formation (e.g., agglomeration, condensation, accretion, fragmentation of larger dust), their respective importance depending on the specific environment.

Already in 1956 John Platt suggested that very small grains or large molecules of less than 1 nm in radius could grow in the ISM by random accretion from the gas (Platt 1956). Today the presence of nanodust in the ISM is generally accepted, but there are still uncertainties in interpreting observations. The discussion in this chapter will focus on the ultrasmall, nanometre-sized interstellar grains. By nanometre-sized grains, or nanodust, we mean grains with a spherical radius of $a \lesssim 10\text{--}20$ nm which undergo stochastic heating and exhibit near-IR and mid-IR emission features in the Galactic ISM (Draine and Li 2001; Li 2004).

For a long time most of our knowledge about interstellar dust was derived from interstellar extinction and reddening, and to a lesser degree from interstellar polarization (which is caused by preferential extinction of one linear polarization over another by aligned nonspherical dust). We will discuss the ISM extinction in the following section. Infrared observations from satellites started in the 1980s and allowed for observing the emission from interstellar dust. The observations indicate the presence of stochastically heated nanodust and emitting polycyclic aromatic hydrocarbon molecules (PAHs) discussed in Sect. 3. Other observational results are also explained with the presence of nanodust: the microwave emission of rotationally excited nanodust (Sect. 4), the photoluminescence of nanodust (Sect. 5), and indirect evidence comes from the photoelectric heating of interstellar gas (Sect. 6). Another population of nanodust are presolar nanograins that are identified in primitive meteorites and collected interplanetary dust and were present in the ISM at the time of the formation of the solar system (Sect. 7). Based on the different

²This mass fraction is much higher for galaxies at early times (since the ISM is gradually consumed by star formation as galaxies evolve) and much lower ($\sim 0.1\%$) for elliptical galaxies. Note that here we do not discuss the observations of nanodust in other galaxies.

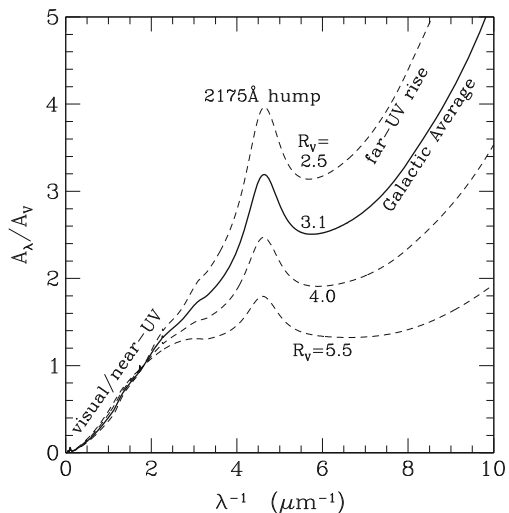
processes that provide evidence for the existence of nanodust in the ISM we then make a comparison to the nanodust in the solar system (Sect. 8) and end with a conclusion. The interstellar extinction and the stochastic heating process are elaborated in Appendixes 1 and 2.

2 The Interstellar Extinction

Small solid dust grains in the ISM absorb and scatter the starlight, so that it appears fainter and redder as expected, this is denoted as interstellar extinction. The Galactic interstellar extinction curves are measured today for various sightlines over a wide wavelength range ($0.1 \mu\text{m} \leq \lambda \leq 20 \mu\text{m}$). Although the extinction curves vary in shape from one line of sight to another, they do exhibit some common appearance (see Fig. 1). The extinction curves are plotted as A_λ/A_V , where A_λ is the extinction, measured in astronomical magnitudes, at wavelength λ and typically given relative to the extinction A_V in the visible wavelength band. The extinction curves shown vs. inverse wavelength λ^{-1} rise almost linearly from the near-infrared (IR) to the near-ultraviolet (UV), with a broad absorption bump at about $\lambda^{-1} \approx 4.6 \mu\text{m}^{-1}$ ($\lambda \approx 2,175 \text{ \AA}$) followed by a steep rise into the far-UV at $\lambda^{-1} \approx 10 \mu\text{m}^{-1}$, the shortest wavelength at which the extinction has been measured.

In the wavelength range of $0.125 \mu\text{m} \lesssim \lambda \lesssim 3.5 \mu\text{m}$, the Galactic extinction curves can be approximated by an analytical formula involving only one free parameter: the total-to-selective extinction ratio, R_V (Cardelli et al. 1989, see Appendix 1). The sightlines through diffuse gas in the Milky Way have $R_V \approx 3.1$ as an average value, but there are considerable regional variations and also the strength and width of the $2,175 \text{ \AA}$ extinction bump vary markedly in the ISM (see Xiang et al. 2011 and

Fig. 1 Interstellar extinction curves of the Milky Way ($R_V = 2.5, 3.1, 4.0, 5.5$). There exist considerable regional variations in the Galactic optical/UV extinction curves, as characterized by the total-to-selective extinction ratio R_V , indicating that dust grains on different sightlines have different size distributions



references therein). Lower-density regions have a smaller R_V , a stronger 2,175 Å bump and a steeper far-UV rise at $\lambda^{-1} > 4 \mu\text{m}^{-1}$, while denser regions have a larger R_V , a weaker 2,175 Å bump and a flatter far-UV rise.

The exact nature of the carrier of this bump remains unknown since its first discovery nearly half a century ago (Stecher 1965). It has been postulated to be nano carbon particles (e.g., Duley and Seahra 1998) or PAHs (Joblin et al. 1992; Li and Draine 2001a; Cecchi-Pestellini et al. 2008; Steglich et al. 2010). Laboratory experiments even suggest that the bump is possibly caused by particles consisting of interplanetary materials (Bradley et al. 2005).

The far-UV part ($\lambda \gtrsim 6 \mu\text{m}^{-1}$) of the Galactic interstellar extinction continues to rise up with shorter wavelength to $\lambda = 0.1 \mu\text{m}$ and there does not appear to be any evidence of saturation even at this wavelength.³ Since it is generally true that a grain absorbs and scatters light most effectively at wavelengths comparable to its size $\lambda \approx 2\pi a$, we can therefore conclude that there must be appreciable numbers of ultrasmall grains with $a \lesssim 0.1 \mu\text{m}/2\pi \approx 16 \text{ nm}$. In the far-UV wavelength range, the grains of a couple of nanometres are in the Rayleigh regime (i.e., $2\pi a/\lambda \ll 1$) and their extinction cross sections per unit volume, $C_{\text{ext}}(a, \lambda)/V$, are independent of size. Hence the far-UV extinction indicates the presence of nanodust, but does not allow to constrain the sizes of the nanodust in the ISM.

3 Emission Brightness from Vibrationally Excited Nanodust and Molecules

The near- and mid-IR⁴ emission of the ISM constrains the size and composition of nanodust, because of its stochastic heating and its characteristic emission in the near-IR. A dust particle in space is subject to substantial temporal fluctuations in temperature, if (1) its heat content is smaller than or comparable to the energy of a single stellar photon (Greenberg 1968) and (2) the photon absorption rate is smaller than the radiative cooling rate (Li 2004). In the diffuse ISM, nanodust is stochastically heated by single photons to temperatures much higher than its “equilibrium” temperature (even though an “equilibrium” temperature is not physical for a stochastically heated nanograin, it can still be *mathematically* determined from the energy balance between absorption and emission).

Figure 2 illustrates the time evolution of grain temperature within a day for PAH/graphite grains exposed to the solar neighbourhood interstellar radiation field (Draine 2003). Grain size decreases from the top to the bottom panel. We see that

³However, the Kramers–Kronig dispersion relation requires that the far-UV extinction rise with inverse wavelengths must turn over at some smaller wavelengths as the wavelength-integrated extinction must be a finite number (see Purcell 1969).

⁴We here use “near-IR” for wavelengths $1 \mu\text{m} \lesssim \lambda \lesssim 12 \mu\text{m}$, “mid-IR” for $12 \mu\text{m} \lesssim \lambda \lesssim 60 \mu\text{m}$ and “far-IR” for $60 \mu\text{m} \lesssim \lambda \lesssim 1,000 \mu\text{m}$.

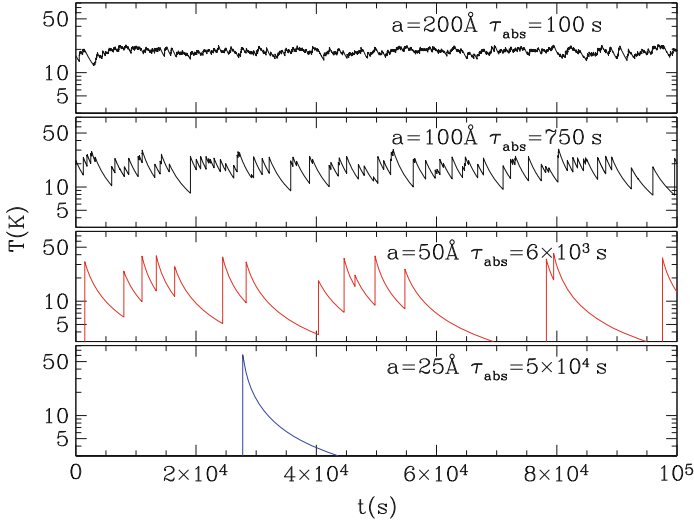


Fig. 2 The time evolution of temperature within a day ($\sim 8.6 \times 10^4$ s) for PAH/graphitic grains of different sizes, a , in the solar neighbourhood interstellar radiation field; τ_{abs} denotes the mean time between photon absorptions. Grains with radii $a \gtrsim 20$ nm have large photon absorption rates $1/\tau_{\text{abs}}$ and large heat capacities so that a single photon cannot significantly alter their temperature. Heat capacities and photon absorption rates are small for grains with radii $a \lesssim 5$ nm and temperature fluctuates strongly. Taken from [Draine \(2003\)](#)

for grain radii $a \gtrsim 20$ nm, individual photon absorptions are relatively frequent, and the grain heat capacity is large enough that the temperature excursions following individual photon absorptions are relatively small; it is reasonable to approximate the grain temperature as being constant in time. Grains with radii $a \lesssim 5$ nm, however, raise their temperature appreciably after absorption of a single photon and since photon absorption rates are small, they can cool down before absorbing another photon. As a result, the temperature raises to well above the mean value. A PAH molecule of 100 carbon atoms (corresponding to a size of ~ 0.6 nm)⁵ will even be heated to $T \approx 785$ K by a photon of $h\nu = 6$ eV, while its “equilibrium” temperature would just be ~ 22 K. The stochastic heating is further discussed in Appendix 2. The grain equilibrium temperatures raise modestly in regions with high photon flux. This is illustrated in Fig. 3 for graphite and silicate grains. When increasing the interstellar radiation field by six times, the particles larger than 10–20 nm increase their equilibrium temperatures by $\sim (6^{1/6} - 1) \approx 35\%$.

Infrared observations from satellites have determined the diffuse ISM brightness for a broad spectral interval (Fig. 4). Initially the emission observed at 12 and 25 μm suggested the presence of nanodust, since it exceeds the emission from large

⁵ The term “PAH size” refers to the radius a of a spherical grain with the same carbon density as graphite (2.24 g cm^{-3}) and containing the same number of carbon atoms N_{C} : $a \equiv 0.13 N_{\text{C}}^{1/3} \text{ nm}$.

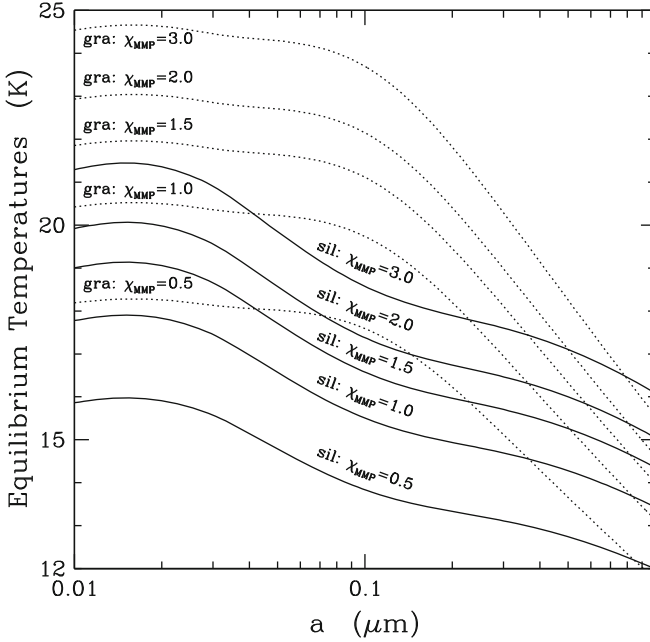


Fig. 3 Equilibrium temperatures for graphite (*dotted lines*) and silicate grains (*solid lines*) in environments with various starlight intensities, χ_{MMP} , in units of the [Mathis et al. \(1983\)](#) solar neighbourhood interstellar radiation field. Grains larger than 10–20 nm attain temperatures 12 K $< T < 25$ K and therefore do not emit appreciably at $\lambda < 60 \mu\text{m}$. Temperatures of grains with $a < 20$ nm do not depend on their size. Taken from [Li and Draine \(2001a\)](#)

grains with ~ 12 – 25 K thermal equilibrium temperature (Fig. 3) by several orders of magnitude ([Boulanger and Perault 1988](#)). Dust emission at 35 and $4.9 \mu\text{m}$ was also detected through broadband photometry ([Arendt et al. 1998](#)). Later observations revealed prominent emission features in the near-IR collectively referred to as the “UIR” bands. The “UIR” features were found at 3.3, 6.2, 7.7, 8.6 and $11.3 \mu\text{m}$ ([Onaka et al. 1996](#); [Tanaka et al. 1996](#); [Mattila et al. 1996](#)) and can be nicely distinguished in Fig. 5. These “UIR” bands are often attributed to PAH molecules ([Leger and Puget 1984](#); [Allamandola 1985](#)). The “UIR” bands alone account already for $\sim 20\%$ of the total IR emission, while the emission at $\lambda \lesssim 60 \mu\text{m}$ accounts for $\gtrsim 35\%$ and that at $\lambda \gtrsim 60 \mu\text{m}$ accounts for $\lesssim 65\%$.

We now discuss a particular model to explain the different ISM dust observations. Figure 5 shows a comparison of the observed emission with the emission calculated from the silicate-graphite-PAH model ([Li and Draine 2001a](#)). In this model, $\sim 15\%$ of the carbon is locked up in the PAH component and the near-IR and “UIR” spectrum are best reproduced by PAHs with a log-normal size distribution peaking at $a \sim 0.6$ nm, corresponding to ~ 100 carbon atoms. At $\lambda \lesssim 60 \mu\text{m}$ the emission is predominantly from PAHs and graphite grains with $a < 25$ nm. Especially the emission at $\lambda = 12, 25 \mu\text{m}$ and shorter wavelengths requires stochastically heated

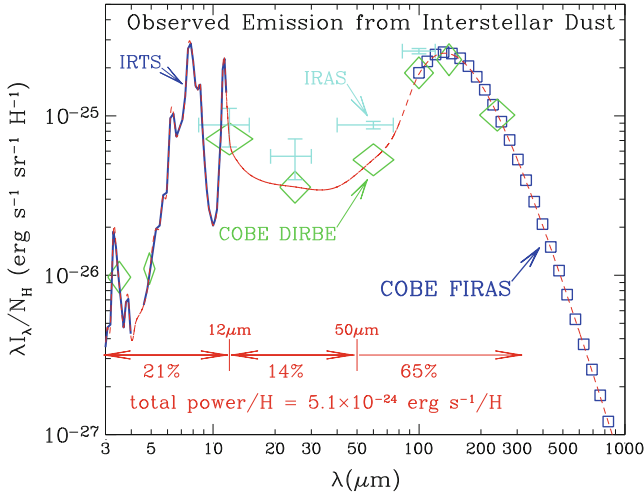


Fig. 4 Observed diffused emission of interstellar dust normalized to the hydrogen column density N_{H} , $\sim 5.1 \times 10^{-24} \text{ erg s}^{-1} \text{ H}^{-1}$. Bars at the *bottom* indicate the relative contributions of the spectral intervals to the total IR emission. The data are from the *Infrared Astronomical Satellite* (IRAS), the *Infrared Telescope in Space* (IRTS), the *Spitzer Space Telescope* (Spitzer) and the *Cosmic Background Explorer* (COBE) satellite with its *Far Infrared Absolute Spectrophotometer* (FIRAS) and its *Diffuse Infrared Background Experiment* (DIRBE). The crosses denote observations from IRAS (Boulanger and Perault 1988), squares from COBE-FIRAS (Finkbeiner et al. 1999), diamonds from COBE-DIRBE (Arendt et al. 1998) and the heavy curve from IRTS (Onaka et al. 1996; Tanaka et al. 1996). Taken from Draine (2003)

nanodust, but even at $\lambda = 60 \mu\text{m}$, the grains with $a < 25 \text{ nm}$ contribute $\sim 70\%$ of the total emission. The model does not include silicate nanodust, since nondetection of the $9.7 \mu\text{m}$ silicate Si–O emission feature in the diffuse ISM (see Fig. 4) indicates its low abundance (see Li and Draine 2001b).

The large silicate and graphite grains of $a > 25 \text{ nm}$ together dominate the emission at $\lambda > 60 \mu\text{m}$, accounting for $\sim 65\%$ of the total IR power. The far-IR emission at $\lambda > 100 \mu\text{m}$ can be closely approximated by a modified blackbody of $I_{\lambda} \propto \lambda^{-\beta} B_{\lambda}(T)$ with $\beta \approx 1.7$ and $T \approx 19.5 \text{ K}$ (see Draine 1999) or by model emission calculated from large grains with $a > 25 \text{ nm}$.

4 Microwave Emission from Rotationally Excited Nanodust

Mappings of the microwave sky have revealed unexpected emission at 10–100 GHz frequencies, as shown in Fig. 6 which basically complements the long wavelength part of the diffuse ISM emission from vibrationally excited, submicrometre-sized dust shown in Fig. 4. The spectral variation and absolute value of this “anomalous” component of the diffuse foreground microwave emission are very different from

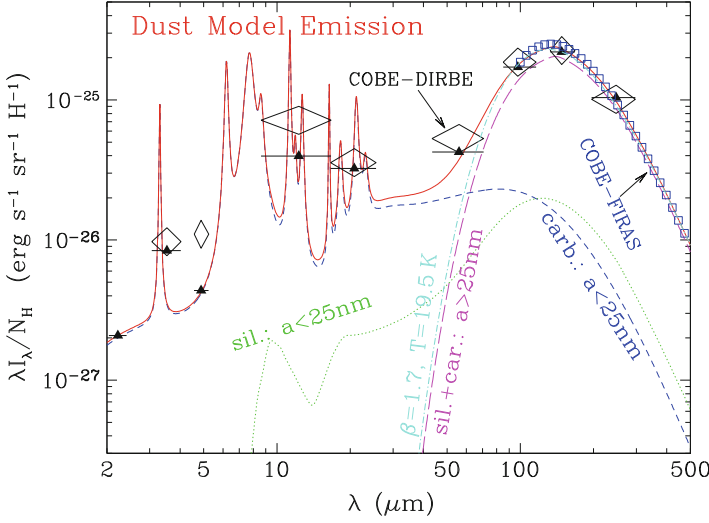


Fig. 5 Calculated dust model emission in comparison to diffuse ISM observations. *Dotted green line*: silicate grains with $a < 25$ nm. *Dashed blue line*: graphite and PAH grains with $a < 25$ nm. *Long dashed magenta line*: the sum of silicate and graphite grains with $a > 25$ nm; *Dot-dashed cyan line*: a modified blackbody of $I_\lambda \propto \lambda^{-\beta} B_\lambda(T)$ with $\beta \approx 1.7$ and $T \approx 19.5$ K approximating the far-IR emission at $\lambda > 100$ μm . The *red solid curve* shows the model spectrum obtained by adding up these different dust emissions. *Triangles* show the latter convolved with the DIRBE filters. *Diamonds* denote observational data from DIRBE (Arendt et al. 1998) and squares from FIRAS (Finkbeiner et al. 1999); see caption to Fig. 4 for the abbreviations. Taken from Li and Draine (2001a)

those of the traditional diffuse emissions at these frequency ranges (e.g., the free-free, synchrotron and thermal dust emission have power-law-like spectra at microwave frequencies) and cannot easily be explained with them.

The spatial distribution of this microwave emission is correlated with interstellar dust emission at 100 and 140 μm (see Draine (2003)), and even better correlated with the mid-IR emission (Casassus et al. 2006; Ysard et al. 2010; Vidal et al. 2011).

This suggests its origins from the dust, but extrapolating the 100–3,000- μm far-IR emission of large dust ($a > 25$ nm) to the microwave frequencies provides values far below the observed microwave emission (see Fig. 6). For these reasons, the electric dipole radiation from rapidly spinning nanograins has become the best explanation for the “anomalous” microwave emission.

A spinning grain with an electric dipole moment μ radiates power $P = 2\omega^4\mu^2 \sin^2\theta/3c^3$, where c is the speed of light and θ the angle between the angular velocity ω and μ . The angular velocity is $\omega = J/I$, where J is the grain angular momentum, and I is the moment of inertia of the grain. It steeply decreases with grain size, since for spherical grains, $I \propto a^5$ and in interstellar environments only nanograins can be driven to rotate fast enough to emit at microwave frequencies. For a PAH grain of

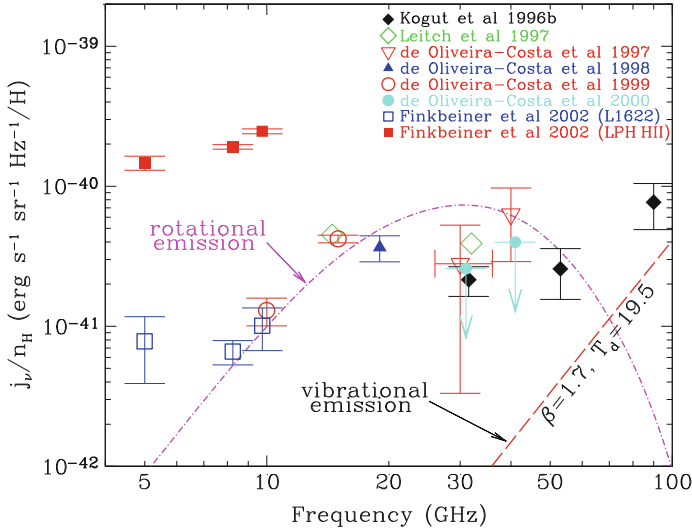


Fig. 6 Galactic foreground microwave emission in comparison to calculated rotational electric dipole emission of the nanograins that account for the “UIR” (see *dashed blue line* in Fig. 5). *Symbols:* observational determinations of “anomalous microwave emission”. *Dot-dashed line:* model rotational emission spectrum of nanodust (Draine and Lazarian 1998). *Dashed line:* low-frequency tail of the emission from large grains (mostly with $a > 25$ nm). Taken from Draine (2003)

radius $a = 1$ nm in the diffuse ISM, J peaks at $\sim 2,000 \hbar$ (see Draine and Lazarian 1998).

As described by Draine and his coworkers (Draine and Lazarian 1998; Hoang et al. 2010), a number of physical processes, including collisions with neutral atoms and ions, “plasma drag” (due to interaction of the electric dipole moment of the grain with the electric field produced by passing ions), and absorption and emission of photons, can drive nanograins to rapidly rotate, with rotation rates reaching tens of GHz. The rotational electric dipole emission from these spinning nanograins, the very same grain component (i.e., PAHs) required to account for the “UIR” emission and the observed 12 and 25- μm continuum emission, was shown to be capable of accounting for the “anomalous” microwave emission (Draine and Lazarian (1998); see Fig. 6). Vidal et al. (2011) found that the microwave emission at 31 GHz of the LDN 1780 translucent cloud correlates better with the 12, 25 μm emission than with the 100 μm emission, which supports that emission at this frequency originates from nanodust.

We should note that although the electric dipole radiation from spinning nanodust provides the best explanation for the “anomalous” microwave emission, other physical mechanisms (e.g., hot free-free emission, hard synchrotron radiation or magnetic dipole emission) could still be contributing at some level (e.g., see Draine 1999; Draine and Lazarian 1999).

5 Extended Red Emission: Photoluminescence from Nanodust

Dust *emission* at optical wavelengths, not expected from its vibrational excitation, is also seen in the red part of the visible spectra of a wide variety of dusty environments. This brightness, which cannot be explained by simple light scattering of dust, is called “extended red emission” (ERE). It is characterized by a broad, featureless band between ~ 540 and 950 nm, with a width of $60 \text{ nm} \lesssim \text{FWHM} \lesssim 100 \text{ nm}$ and a peak of maximum emission at $610 \text{ nm} \lesssim \lambda_p \lesssim 820 \text{ nm}$, depending on the physical conditions of the environment where the ERE is produced (see Fig. 7). The peak wavelength λ_p varies from source to source and within a given source with distance from the illuminating star. The ERE width appears to increase as λ_p shifts to longer wavelengths (Darbon et al. 1999). The ERE has been seen in various different regions which, in terms of UV photon densities, span a range of six orders of magnitudes and, in terms of dust, represent both heavily processed interstellar dust, as well as relatively “freshly” produced dust (e.g., see Witt and Vijh 2004).

The ERE is commonly attributed to photoluminescence (PL) by some component of interstellar dust, a process in which absorptions of UV photons are followed by electronic transitions associated with the emission of optical or near-IR photons. For a given material the wavelength of photoluminescence varies with the size of the grains. The ERE is powered by UV/visible photons, as demonstrated by Smith and

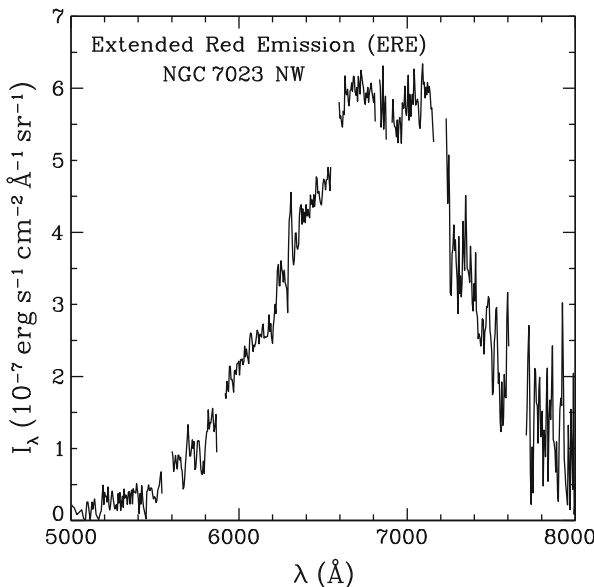


Fig. 7 Observed photoluminescence spectrum—the “extended red emission” (ERE) arising from an unidentified nanodust species in the north-west (NW) filament of NGC 7023, a reflection nebula. Data taken from Witt and Vijh (2004)

Witt (2002) who found that the maximum ERE intensity in any given environment is closely correlated with the density of UV photons.

The true nature of the ERE carriers still remains unknown, although over a dozen candidates have been proposed over the past decades. For a proposed candidate to be valid, it must luminesce in the visible with its spectrum matching that of the observed ERE. But this is not sufficient. As many candidate materials luminesce in the visible after excitation by UV photons, along with the carrier abundance, the efficiency for photoluminescence—the quantum efficiency for the conversion of UV photons absorbed by the ERE carrier to ERE photons—represents one of the strongest constraints.

Gordon et al. (1998) placed a lower limit on the photon conversion efficiency η_{PL} (measured by the number ratio of luminesced photons to exciting UV photons) to be approximately $(10 \pm 3)\%$ (also see Szomoru and Guhathakurta 1998). This lower limit was derived from the correlation of ERE intensity with HI (neutral hydrogen) column density at high Galactic latitudes (Gordon et al. 1998), with the assumption that *all UV absorption is due to the ERE carrier candidate* (in other words, assuming that *all the UV photons absorbed by dust lead to the production of ERE*). Since other absorbing interstellar dust components, not likely associated with ERE, are known, the actual luminescing efficiency must be substantially larger than 10%, perhaps in the vicinity of 50% or even higher (Smith and Witt 2002). This poses a serious challenge to materials once thought to be promising ERE candidates, as their luminescing efficiencies are $<1\%$ (see Wada et al. 2009; Godard and Dartois 2010).

All these suggest that the ERE carriers are very likely in the nanometre size range because (a), in general, nanograins are expected to luminesce efficiently through the recombination of the electron–hole pair created upon absorption of an energetic photon, since in such small systems the excited electron is spatially confined and the radiationless transitions that are facilitated by Auger- and defect-related recombination are reduced and (b) small nanograins may be photolytically more unstable and/or more readily photoionized in regions where the radiation intensity exceeds certain levels of intensity and hardness, and thus resulting in both a decrease in the ERE intensity and a redshift of the ERE peak wavelength.⁶ Observationally, Darbon et al. (1999) and Smith and Witt (2002) showed that the ERE peak wavelength is indeed shifted towards longer wavelengths with increasing UV radiation density.

Several materials have been proposed as ERE carriers: carbon nanoparticles (Seahra and Duley 1999), silicon nanoparticles (Witt et al. (1998); Ledoux et al. (1998); but see Li and Draine (2002)), nanodiamonds (Chang et al. 2006) and

⁶This is because (1) photoionization would reduce the luminescence of nanograins and (2) the smaller grains would be selectively removed due to size-dependent photofragmentation (Smith and Witt 2002). Due to the quantum confinement effect, the band gap of a semiconductor-like nanograin is *smaller* (and therefore the wavelength of luminescing photons is *longer*) for a *bigger* nanograin (see Sect. 4 in Li 2004).

PAH clusters (Berné et al. 2008). But none of them satisfies all the observational requirements (see Li 2004).

6 Photoelectric Heating of the ISM Gas by Nanodust

Observations of the 21 cm line⁷ show that the diffuse neutral atomic hydrogen gas (HI) in the ISM is in two distinct phases with temperatures ~ 100 K (“Cold Neutral Medium”) and $\sim 6,000$ K (“Warm Neutral Medium”). What heats the gas to temperatures of ~ 100 or $\sim 6,000$ K? One possible answer to this question provides indirect evidence for the existence of an appreciable quantity of nanodust in the ISM. It has long been recognized that photoelectrons ejected from grains heat the interstellar gas: After absorbing photons with sufficiently large energy, the dust emits photoelectrons, which transfer kinetic energy through inelastic collisions to the gas.

The photoelectrons are important for heating the gas because (a) photons with energies below the ionization potential of H (~ 13.6 eV) do not couple directly to the gas and (b) other heating sources such as cosmic rays, magnetic fields and turbulence are not important as a global heating source for the diffuse ISM (e.g., the cosmic ray flux is too low by a factor of ~ 10 to account for the interstellar gas heating; Watson 1972).

In the diffuse ISM, nanodust (and, in particular, angstrom-sized PAH molecules) are much more efficient in heating the gas than large grains (see Tielens 2008) since (a) the mean free path of an electron in a solid is just ~ 1 nm and therefore photoelectrons created inside a large grain rarely reach the grain surface and (b) the total far-UV absorption is dominated by the nanodust component (see Sect. 3). Theoretical studies have shown that grains smaller than 10 nm are responsible for $\gtrsim 96\%$ of the total photoelectric heating of the gas, with half of this provided by grains smaller than 1.5 nm (Bakes and Tielens 1994; Weingartner and Draine 2001b). Figure 8 shows the calculated photoelectric heating rate as a function of grain size. The size is quantified by the number, N_C of carbon atoms and by the graphite-equivalent spherical radius $a \sim 0.13 N_C^{1/3}$ nm.

Observations confirm the dominant role of nanodust in the gas heating through the photoelectric effect. For instance, Habart et al. (2001) studied the major cooling lines, [CII] 158 μm and [OI] 63 μm , of L 1721, an isolated cloud illuminated by a B2 star in the ρ Ophiuchi molecular complex. Because of the energy balance between heating and cooling, the [CII] 158 μm and [OI] 63 μm cooling lines (which dominate the gas cooling) reflect the heating input to the gas. They found that the spatial distributions of the gas cooling lines closely correlate with that of the mid-IR emission attributed to nanodust (and PAHs).

⁷The 21-cm line originates in the hyperfine splitting of the parallel and antiparallel spin states of the electron (relative to the spin of the proton) in the electronic ground state ($1s$) of atomic H.

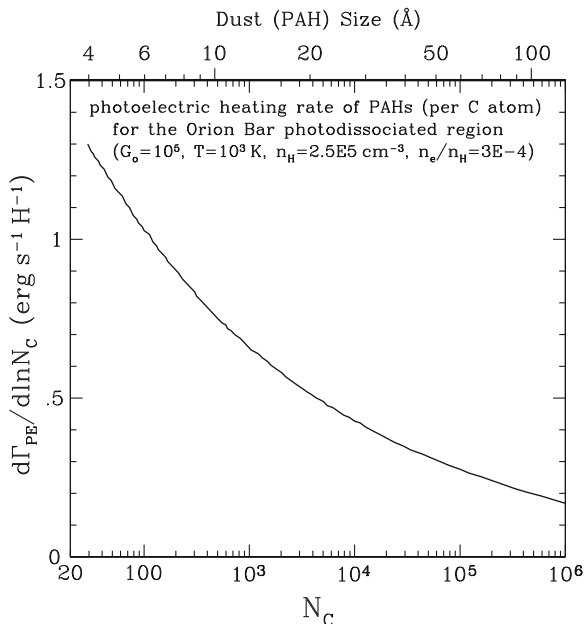


Fig. 8 The photoelectric heating rate Γ_{PE} of the interstellar gas in the Orion Bar photodissociated region as a function of PAH size. The lower axis shows the number, N_C of carbon atoms and the upper axis the graphite-equivalent spherical radius. The rates are presented in such a way that equal areas under the curve correspond to equal contributions to the heating. Typically, approximately half of the heating originates from PAHs and PAH clusters (with $N_C < 10^3$ or $a < 1.3$ nm). The other half comes from grains with sizes $1.3 \text{ nm} < a < 10 \text{ nm}$. Larger grains do not contribute noticeably to the heating. Data taken from [Bakes and Tielens \(1994\)](#)

7 Direct Evidence: Presolar Nanodust in Primitive Meteorites

Based on their isotopic anomalies, presolar grains (such as graphite, silicate, silicon carbide SiC, silicon nitride Si₃N₄, and refractory oxides including corundum Al₂O₃, spinel MgAl₂O₄) that predate the solar system have been identified in primitive meteorites, a class of meteorites that essentially remained chemically unaltered since their formation in the solar nebula (e.g., see [Lodders 2005](#)). Their path from formation to detection in the laboratory is sketched in Fig. 9, which also shows examples for the two observed nanometre-sized grain types.

Presolar nanodiamonds of radii $a \sim 1$ nm were found to be rich in primitive carbonaceous meteorites, with an abundance as much as $\sim 0.1\%$ of the total mass in some primitive meteorites, more abundant than any other presolar grains by

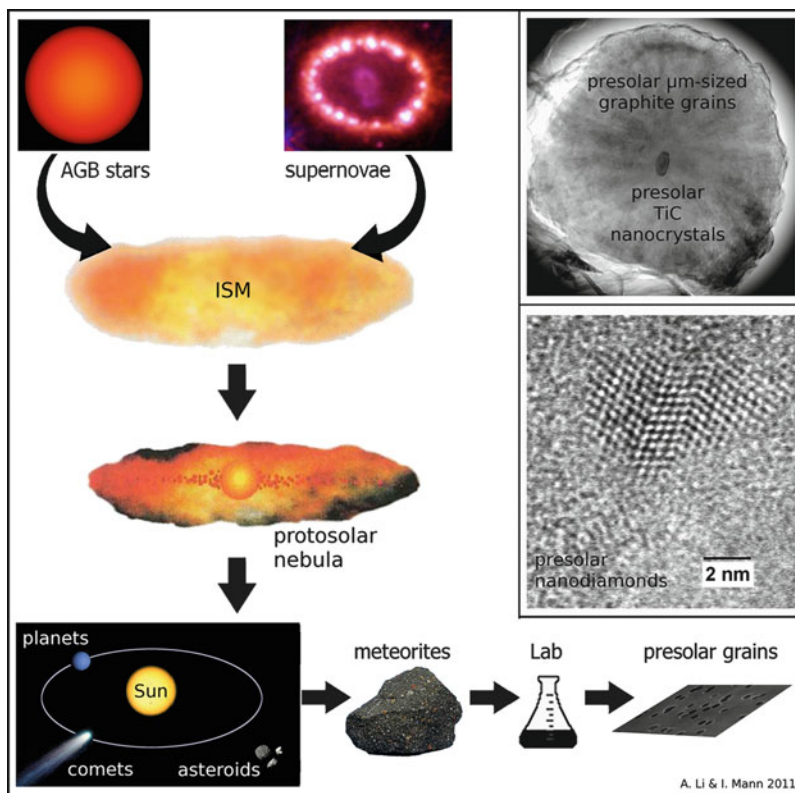


Fig. 9 A schematic illustration of the history of presolar grains from their condensation in stellar winds of *asymptotic giant branch* (AGB) stars or in supernova ejecta to our solar system. These grains survived all the violent processes occurring in the ISM and in the early stages of solar system formation and were incorporated into meteorite parent bodies, from which they are extracted in the laboratories. Inserted are the *transmission electron microscopy* (TEM) images of presolar nanodiamond grains (Banhart et al. 1998) and a presolar TiC nanocrystal within a micrometer-sized presolar graphite spherule (Bernatowicz et al. 1991)

over two orders of magnitude (Lewis et al. 1987).⁸ Presolar titanium carbide (TiC) nanocrystals were also seen in primitive meteorites. With a mean radius of ~ 3.5 nm, they occur as nanometre-sized inclusions within micrometer-sized presolar graphitic spherules (Bernatowicz et al. 1991).

These presolar nanograins, after their condensation in stellar outflows from carbon-rich evolved stars (e.g., TiC nanocrystals) or in ejecta from supernova explosion (e.g., nanodiamonds), and prior to their incorporation into the parent

⁸The identification as presolar grains by measuring isotope ratios does not work for single nanodiamonds and there is a debate whether a fraction of them may actually have formed after the formation of the solar system (e.g., see Ott 2007).

bodies of meteorites during the early stages of solar system formation, they must have had a sojourn in the ISM out of which the solar system formed. However, neither nanodiamonds nor TiC nanocrystals could be representative of the bulk composition of nanodust in the ISM (Draine 2003).

8 Summary and Comparison to Nanodust in the Solar System

Based on the discussions in the previous sections we can summarize the major observational evidence for the presence of nanodust in the ISM: (1) the far-UV extinction at $\lambda^{-1} > 6 \mu\text{m}^{-1}$ caused by the absorption of nanodust (Sect. 2), (2) the $\sim 2\text{--}60 \mu\text{m}$ near- and mid-IR spectral and continuum emission from stochastically heated nanograins through vibrational relaxation (Sect. 3), (3) the $\sim 10\text{--}100 \text{ GHz}$ “anomalous” Galactic foreground microwave emission from rotationally excited nanograins through electric dipole radiation (Sect. 4) and (4) the $\sim 5,400\text{--}9,500 \text{ \AA}$ broad, featureless ERE band from electronically excited nanograins through photoluminescence (Sect. 5). The presence of an appreciable amount of nanograins in the ISM is also indirectly inferred from the photoelectric heating of interstellar gas by nanodust (i.e., PAHs; Sect. 6) and finally presolar grains are found in interplanetary dust and meteorites of the solar system. Our list is not complete. The nanodust population (particularly PAHs) may also be responsible for the lower gas-phase deuterium abundance of $\text{D}/\text{H} \approx 7\text{--}22 \text{ ppm}$ in the Galactic ISM compared to the primordial value of $\text{D}/\text{H} \approx 26 \text{ ppm}$, through depleting the “missing” D onto PAHs (Draine 2006).

Based on the preceding discussion the physical processes that allow the direct or indirect observation of nanodust are UV light-scattering, stochastic heating, electric dipole radiation of rotating nanodust, photoluminescence and finally photoelectric heating of the surrounding gas.

We now discuss the possible occurrence of these processes in the solar system. It is worth noting at the beginning that the nanodust in the solar system is not identical to the nanodust in the ISM. The grains with $a < 5 \text{ nm}$ in the local interstellar cloud in the vicinity of the Sun do not enter the solar system, as they are deflected by the magnetic field that builds up in the outer solar system due to interaction of the local ionized ISM gas with the solar wind (Mann 2010). The nanodust in the solar system is produced locally from the interplanetary dust cloud or from solar system objects.

- *Light-scattering in far UV:* Scattering from interplanetary dust particles generated the Zodiacal light, which is the predominant diffuse brightness of the night sky to wavelengths as short as $\lambda \sim 0.3 \mu\text{m}$. In contrast to the dust in the ISM, the geometric cross section of the dust size distribution in the interplanetary medium has its maximum in the $1\text{--}100\text{-}\mu\text{m}$ interval and smaller dust contributes only little to the observed brightness. This is supported by the red colour of the Zodiacal light relative to the solar spectrum (Pitz et al. 1979), which does

not indicate any significant contribution from light scattered by nanodust. The brightness at shorter wavelength is dominated by the emission of unresolved stars (Leinert et al. 1998). Dust emission in the X-ray was discussed after the ROSAT survey established comets as a class of X-ray sources. The discussed dust-related X-ray signals are X-ray fluorescence and scattering by nanodust and X-ray emission caused by high-velocity impacts of nanodust. The X-ray flux from nanodust in the solar system is estimated by Kharchenko and Lewkow in this book.

- *Stochastic heating:* For the nanograins in the inner solar system (Mann et al. 2007), it is more likely for them to attain an equilibrium temperature (compared to the same dust in the diffuse ISM). This is because the solar system nanodust is exposed to a far more intense radiation field: at distance r_h from the Sun, the 912 \AA – $1\text{-}\mu\text{m}$ solar radiation intensity is $\approx 7.6 \times 10^7 (r_h/\text{AU})^{-2}$ times that of the local interstellar radiation field, where r_h is the distance from the Sun. Figure 10 shows the temperature probability distribution functions of amorphous silicate dust using the dielectric functions of Draine and Lee (1984) for selected sizes ($a = 3.5 \text{ \AA}$, 5 \AA , 1 nm , 2 nm , 5 nm) illuminated by the Sun at $r_h = 0.1, 1 \text{ AU}$. To facilitate comparison, we plot $dP/d \ln T$ in the same T and $dP/d \ln T$ ranges for $r_h = 0.1 \text{ AU}$ and $r_h = 1 \text{ AU}$. The emission is also illustrated in the same λ and j_λ ranges (except the latter differs by a factor of r_h^{-2}). We see that silicate dust with $a \gtrsim 2 \text{ nm}$ attains an equilibrium temperature of $T_{\text{eq}} \approx 282 \text{ K}$ at $r_h = 1 \text{ AU}$. At $r_h = 0.1 \text{ AU}$, the $dP/d \ln T$ distribution functions for grains as small as $a = 1 \text{ nm}$ are already like a delta function, peaking at $T_{\text{eq}} \approx 1,081 \text{ K}$. At $r_h = 1 \text{ AU}$, the silicate emission spectra for $a = 2, 3, 5 \text{ nm}$ are almost identical. This is because in the entire UV to far-IR wavelength range, these nanograins are in the Rayleigh regime and their Q_{abs}/a values are independent of size, therefore they obtain an almost identical equilibrium temperature. At $r_h = 0.1 \text{ AU}$, this even applies to smaller grains (e.g., $a = 1 \text{ nm}$). To summarize, in the solar system at $r_h < 1 \text{ AU}$, the stochastic heating effect is small for dust larger than $\sim 1 \text{ nm}$ in radius; for dust smaller than $\sim 5 \text{ \AA}$, it may not survive since the stochastic heating would lead to temperatures exceeding $\sim 2,000 \text{ K}$. This is roughly the sublimation temperature of silicate dust, though we point out that the nanodust can have lower sublimation temperature than the bulk material (see Kimura, 2012 in this book).
- *Electric dipole radiation of rotating dust:* We are not aware of any studies of the rotational dynamics of nanodust in the solar system. We do not expect to see strong microwave emission from the dust in the solar system. Although the ions in the solar system may deliver more angular momentum to a grain than in the diffuse ISM (because of their large abundance and large kinetic energy), the dust will not be driven to rotate as fast as in the diffuse ISM, due to (1) the large grain size of the solar system nanodust population, (2) the strong rotational damping caused by photon emission in the solar system and (3) the small number densities of nanodust in the directions facing away from the Sun (see other chapters of this book). The nanodust in the solar system seems to be in the nm size range (see other chapters of this book), while the microwave emission in the ISM arises predominantly from angstrom-sized PAHs. Note that the angular velocity $\omega \propto 1/I$, while $I \propto a^5$.

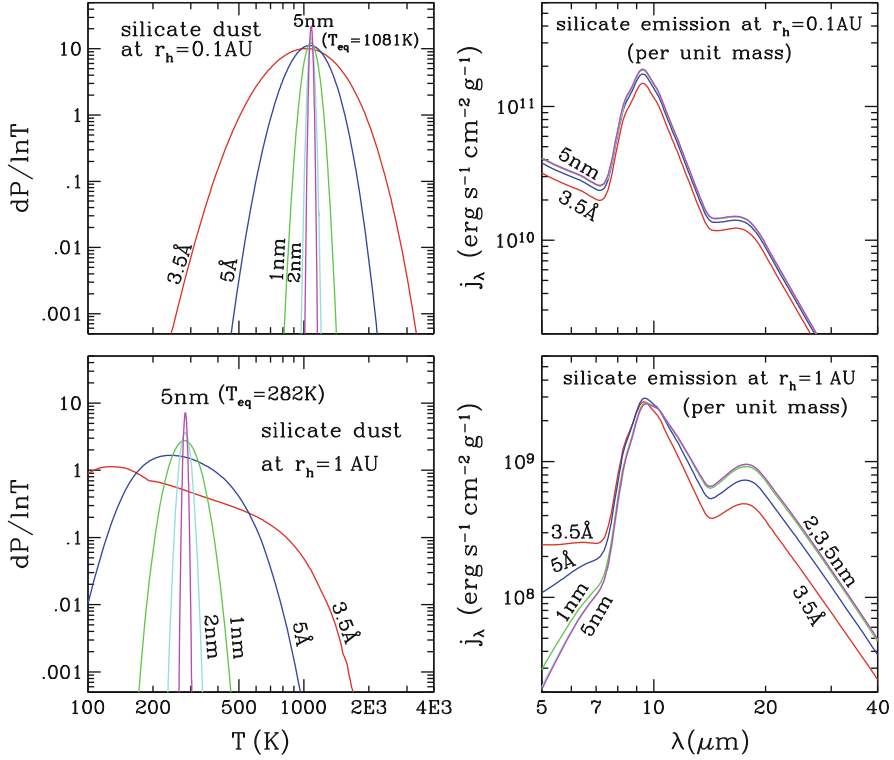


Fig. 10 Temperature probability distribution $dP/d\ln T$ and emission for silicate grains at distances $r_h = 0.1, 1$ AU from the Sun. The distributions at $r_h = 1$ AU are much broader than that for the same dust at $r_h = 0.1$ AU. The grains with $a > 1$ -nm peak at the same temperature (which is their equilibrium temperature), as expected from their Rayleigh scattering nature (see Sect. 8)

- *Photoluminescence*: As far as observations in the solar system are concerned a coronal emission that appeared similar to the ERE was speculated to result from silicon nanocrystals near the Sun (Habbal et al. 2003), but this was challenged on the basis of the dust composition and emission properties (Mann and Murad 2005). As opposed to the ISM the nanodust in the solar system most likely is heterogeneous in composition and covers a broad size interval. This broadens wavelength at which the photoluminescence is observed, which makes its detection near the Sun less likely. At this point, we are not aware of an observational result in the optical or IR range confirming the existence of nanodust in the solar system and the detection of nanodust in the interplanetary medium in a similar way like the ERE is unlikely (see Mann and Czechowski, 2012 in this book).
- *Photoelectric heating*: For the solar system nanodust, photoelectric heating does not occur because the nanodust is embedded in the high temperature solar wind electrons. Instead, the presence of nanodust in the solar wind would rather lead to

cooling, because the solar wind ions charge-exchange and are decelerated when passing a nanograin.

9 Conclusion

Observational data, particularly the near- and mid-IR emission data, allow us to constrain the composition, size distribution and quantity of the nanodust population in the ISM: (1) PAHs and nanometre-sized graphitic grains are the dominant nanodust species in the ISM; they contain $\sim 15\%$ of the total interstellar carbon, produce the IR emission at $\lambda < 30\ \mu\text{m}$ (including the “UIR” bands) as well as the microwave emission; (2) Nano silicate grains are not important: they *at most* account for $\sim 5\%$ of the total interstellar silicon as indicated by the nondetection of the $9.7\text{-}\mu\text{m}$ silicate Si–O emission band in the Galactic diffuse ISM (Li and Draine 2001b). Presolar nanograins (i.e., nanodiamonds and TiC nanocrystals) that are identified in primitive meteorites and interplanetary dust are not an abundant population of the ISM nanodust, but provide the most direct evidence for interstellar nanodust. They were present in the local ISM at the time of the formation of the solar system. The physical processes involving nanodust in the ISM are less important for the nanodust in the solar system. Nonetheless, considering the stochastic heating process suggests that the size of the silicate nanodust in the inner solar system is possibly constrained by sublimation.

Appendix 1: Interstellar Extinction

The existence of small solid dust grains in interstellar space was established in 1930 when Trumpler showed that the stars in distant open clusters appear fainter than could be accounted for just by the inverse square law, and many stars in the galactic plane appear redder than expected from their spectral types; he interpreted these observations in terms of interstellar extinction and selective absorption (i.e., reddening) caused by “fine cosmic dust particles of various sizes” (Trumpler 1930).

The interstellar extinction curve is most commonly derived utilizing the “pair” method. As illustrated in Fig. 11, this technique involves photometric or spectrophotometric observations of two stars of identical spectral types, with one star located behind a dust cloud and another star (in ideal case) unaffected by interstellar dust, so that there is no obscuration between the observer and the star. Let F_λ be the observed flux from the reddened star, and $F_{o,\lambda}$ be the flux from the unreddened star. If both stars are located at an identical distance, the extinction A_λ —measured in “magnitudes”—is

$$A_\lambda \equiv 2.5 \log_{10} [F_{o,\lambda} / F_\lambda] \approx 1.086 \tau_\lambda, \quad (1)$$

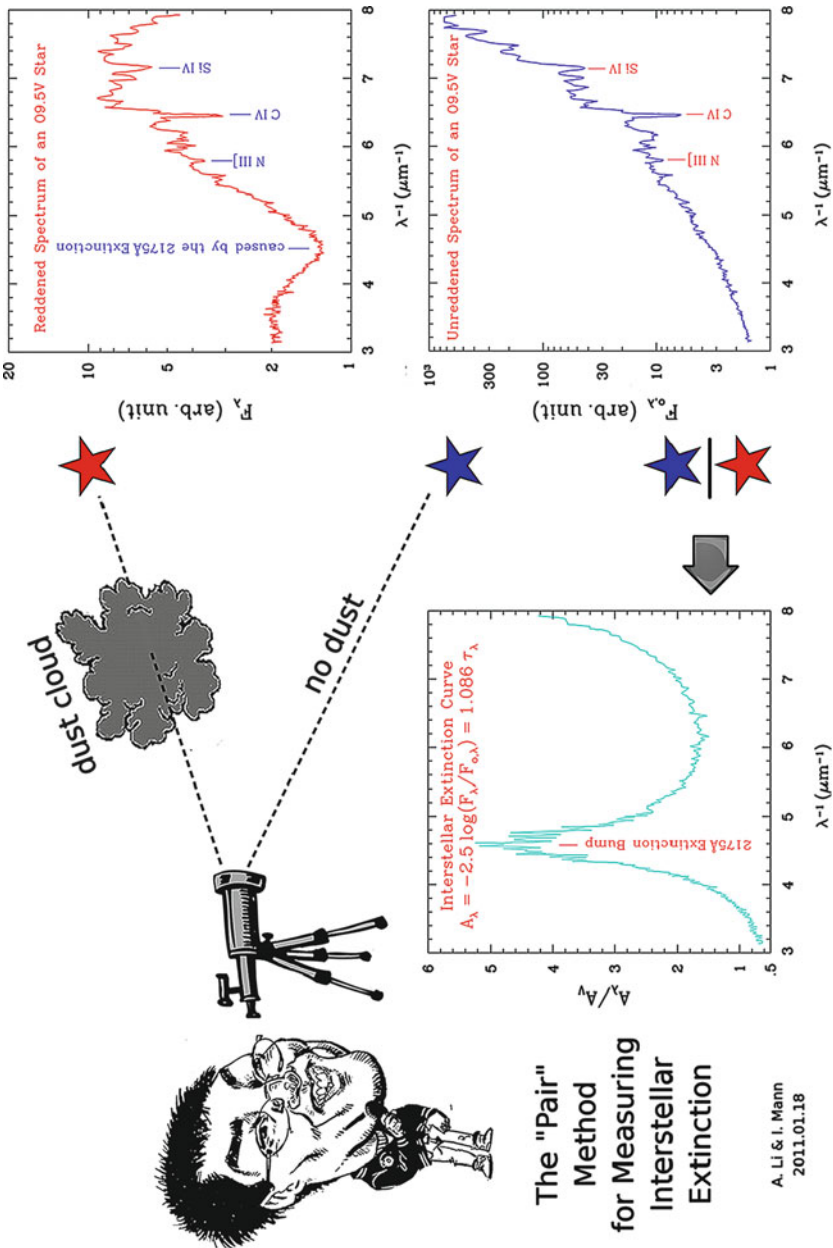


Fig. 11 A conceptual illustration of the "pair" method

where τ_λ is the optical depth. For the ISM within a few kilo pc from the Sun within the Galactic plane and within ~ 100 pc of the galactic plane, the mean visual extinction per unit path-length has long been determined quite accurately to $\langle A_V/L \rangle \approx 1.8 \text{ mag kpc}^{-1}$ (e.g., see [Kapteyn 1904](#)).

As it is often not possible to find reddened/unreddened star pairs of identical spectral types which are also located at identical distances, one often measures the colour excess

$$E(\lambda - V) \equiv A_\lambda - A_V = 2.5 \log_{10} \left[\frac{F_{\lambda, \lambda}/F_{\lambda, V}}{F_\lambda/F_V} \right] \quad (2)$$

from normalized stellar fluxes, with the V band being the usual choice for the normalization purpose. The total-to-selective extinction ratio

$$R_V \equiv A_V/E(B - V) \quad (3)$$

suggested by [Cardelli et al. \(1989\)](#) is frequently used to characterize the galactic extinction curves.

For particles in the Rayleigh regime (i.e., $2\pi a/\lambda \ll 1$) their extinction cross sections per unit volume, $C_{\text{ext}}(a, \lambda)/V$, are independent of size. Therefore, the observational quantity A_λ/N_H ($\text{mag cm}^{-2} \text{H}^{-1}$)—the extinction per unit H column—only constrains V_{tot}/n_H , the total dust volume per H nuclei of this grain component:

$$A_\lambda/N_H = 1.086 \int C_{\text{ext}}(a, \lambda) n_H^{-1} (dn/da) da = 1.086 (V_{\text{tot}}/n_H) (C_{\text{ext}}/V), \quad (4)$$

where dn is the number of grains in the size interval $[a, a + da]$, and N_H (n_H) is the hydrogen column (volume) density. This explains why the MRN silicate–graphite model with a lower size cut-off of $a_{\text{min}} = 5 \text{ nm}$ ([Mathis et al. 1977](#)), which was frequently used before the presence of nanodust was confirmed, could also closely reproduce the observed extinction curve. The MRN model fitted the extinction curve using a mixture of silicate and graphite grains with a simple power-law size distribution: $dn/da \propto a^{-3.5}$ for $5 \text{ nm} \lesssim a \lesssim 0.25 \text{ } \mu\text{m}$.

The $2,175 \text{ } \text{\AA}$ bump is thought to be predominantly due to absorption, as indicated by the broad minimum near $2,175 \text{ } \text{\AA}$ of the interstellar albedo ([Whittet 2003](#)). The interstellar albedo is defined as the ratio of scattering to extinction. The interstellar extinction is the combination of scattering and absorption. For grains in the Rayleigh limit, the scattering is negligible in comparison with the absorption (see [Li 2009](#)). This suggests that its carrier is sufficiently small to be in the Rayleigh limit, with a size $a \ll \lambda/2\pi \approx 35 \text{ nm}$.

Finally, we should note that a smooth extension of the MRN $dn/da \propto a^{-3.5}$ size distribution down to $a = 3 \text{ } \text{\AA}$ is not sufficient to account for the observed $12 \text{ } \mu\text{m}$ and $25\text{-} \mu\text{m}$ emission (see [Draine and Anderson 1985](#); [Weiland et al. 1986](#)) and that an extra population of nanometre-sized dust is required (e.g., see [Désert et al. 1990](#); [Dwek et al. 1997](#); [Li and Draine 2001a](#)). In the recent [Weingartner and Draine](#)

(2001a) model, for instance, the grain size distribution extends from a few angstroms to a few micrometers, with $\sim 6\%$ of the total dust mass in grains smaller than 2 nm.

Appendix 2: Stochastic Heating

Typically large dust particles in the interstellar medium reach equilibrium temperature for which the rate of radiative cooling equals the time-averaged rate of energy absorption. If the emissivity of the dust material is roughly constant with wavelength (which is more the case for a large particle) then the spectral slope of the thermal emission brightness is roughly that of a blackbody (Planck curve) with the location of maximum emission being determined by the temperature (i.e., modified blackbody or grey body). For interpreting astronomical observations a dust temperature is often assumed to be the equilibrium temperature and one denotes as colour temperature of an object the temperature of a blackbody with peak emission at the same wavelength as the observed brightness. The required dust (colour) temperature to generate peak emission in the mid-IR is, for instance, ~ 300 K for the 12- μm emission and ~ 150 K for the 25- μm emission. For temperatures of nanodust, in contrast, the Debye model more adequately considers a finite number of vibrational states of the atomic lattice to calculate emission. The Debye temperature Θ (with a dimension of kelvin) characterizes the low-temperature heat capacity U of a solid.

Nanograins are small enough that their time-averaged internal energy is smaller than or comparable to the energy of the starlight photons that heat the grains. Stochastic absorption of photons therefore results in transient “temperature spikes”, during which much of the energy deposited by the starlight photon is reradiated in the near- or mid-IR.

The “temperature spike”—the maximum temperature to which a nanograin can reach upon an absorption of a photon, is sensitive to its heat capacity (which is $\propto a^3$). When illuminated by a radiation field, the observed intensity I_λ from the transiently heated nanograins is

$$I_\lambda = N_H \int C_{\text{abs}}(a, \lambda) n_H^{-1} (dn/da) da \int B_\lambda(T) (dP/dT)_a dT, \quad (5)$$

where $C_{\text{abs}}(a, \lambda)$ is the absorption cross section for a grain of radius a at wavelength λ , $B_\lambda(T)$ is the Planck function at temperature T and $(dP/dT)_a$ is the dust temperature distribution function which is sensitive to grain size a (see Li 2004). We see that although in the IR wavelength range $C_{\text{abs}}(a, \lambda)/V$ is independent of grain size a , $(dP/dT)_a$ is a sensitive function of a and therefore I_λ allows us to constrain the size distribution of the nanodust component through $(dP/dT)_a$.

Figure 12 shows the temperature probability distributions $dP/d \ln T$ for PAH ions of selected sizes (at $a > 5$ nm their optical properties approach that of graphite; see Li and Draine 2001a). The distributions are shown for $\chi_{\text{MMP}} = 1$

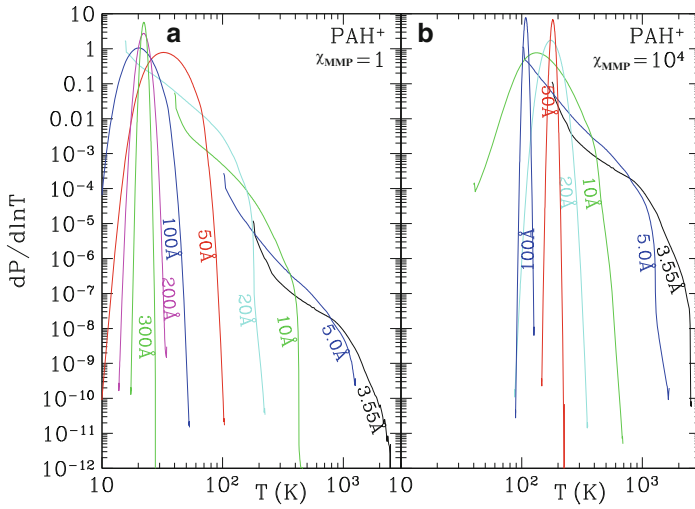


Fig. 12 Temperature probability distribution $dP/d \ln T$ for selected PAH ions heated by starlight with $\chi_{\text{MMP}} = 1$ and $\chi_{\text{MMP}} = 10^4$ (in unit of the MMP local interstellar radiation field). It is interesting to note that in the case of $\chi_{\text{MMP}} = 1$, the $a = 20$ nm grain and the $a = 30$ nm grain (even the $a = 10$ nm grain as well) peak at the same temperature (which is their equilibrium temperature). This is expected from their Rayleigh scattering nature (see the caption of Fig. 3). However, in the case of $\chi_{\text{MMP}} = 10^4$, the $a = 5$ nm grain and the $a = 10$ nm grain do not peak at the same temperature, although they both attain equilibrium temperatures. This is because they were “designed” to have different optical properties: PAHs with $a \gtrsim 10$ nm have graphitic properties, while those with $a \lesssim 5$ nm have PAH properties (see Li and Draine 2001a). Taken from Draine and Li (2007)

and $\chi_{\text{MMP}} = 10^4$, where χ_{MMP} is the starlight intensity in units of the interstellar radiation field given by Mathis et al. (1983) (MMP). We see in Fig. 12a that small grains undergo extreme temperature excursions (e.g., the $a = 3.55$ Å PAH occasionally reaches $T > 2,000$ K), whereas larger grains (e.g., $a = 30$ nm) have temperature distribution functions that are very strongly peaked and like a delta-function, corresponding to only small excursions around an equilibrium temperature. It is apparent that when the rate of photon absorption increases, the “equilibrium” temperature approximation becomes valid for smaller grains; e.g., for $\chi_{\text{MMP}} = 10^4$ one could approximate a $a = 5$ -nm grain as having an equilibrium temperature $T_{\text{eq}} \approx 150$ K whereas for $\chi_{\text{MMP}} = 1$ the temperature excursions are very important for this grain (see Draine and Li 2007). This is also the reason for stochastic heating not being important in the inner solar system.

Whether a grain will undergo stochastic heating depends on (1) the grain size, (2) the optical properties of the dust, (3) the thermal properties (e.g., Debye temperature) of the dust, (4) the starlight intensity, and (5) the hardness of the starlight, which measures the relative amount of short-wavelength (“hard”) photons compared to long-wavelength (“soft”) photons. For a *smaller* grain with a *smaller* UV/visible absorptivity and a *larger* Debye temperature Θ , exposed to starlight

of a *lower* intensity and a *harder* spectrum, it is *more* likely for this grain to be stochastically heated by single photons. This is because (1) the specific heat of a grain (at a given temperature) is proportional to a^3/Θ^3 , a single photon (of a given energy) would therefore result in a *more* prominent temperature spike for a *smaller* grain with a *larger* Θ ; (2) the photon absorption rate is proportional to the starlight intensity and the absorptivity of the dust in the UV/visible wavelength range, a *smaller* grain with a *smaller* UV/visible absorptivity when exposed to a more *dilute* radiation field will have a *smaller* photon absorption rate and will therefore more likely undergo stochastic heating; (3) a *more* energetic photon would cause a grain to gain a *larger* temperature raise, grains are therefore *more* likely to experience transient heating when exposed to a *harder* radiation field.

Before the stochastically heated nanodust was observed in the diffuse ISM, it was already seen in some other objects. Andriesse and de Vries (1976) presented the first IR emission evidence for nanodust in the dust cloud in M 17, a star-forming nebula. They found that the 8–20- μm emission spectrum is similar over a distance of $\sim 2'$ through the source, suggesting a constant dust temperature. Since large, submicron-sized grains would attain equilibrium temperatures that decrease with distance from the illuminating source, Andriesse (1978) interpreted this as due to stochastically heated grains of $\sim 1\text{ nm}$. A more definite piece of observational evidence was provided by Sellgren et al. (1983) who observed three visual reflection nebulae, clouds of dust that scatter the light of nearby stars, their near-IR observations (at 1.25–4.8 μm) consisting of emission features at 3.3 and 3.4 μm and a smooth continuum characterized by a colour temperature $\sim 1,000\text{ K}$. Both the 3.3- μm feature and the colour temperature of the continuum show very little variation from source to source and within a given source with distance from the central star. Sellgren (1984) argued that this emission could not be explained by thermal emission from dust in radiative equilibrium with the central star since otherwise the colour temperature of this emission should fall off rapidly with distance from the illuminating star; instead, she proposed that this emission is due to stochastically heated nanodust.

Acknowledgements We thank M. Köhler for her great help in preparing for Figs. 9 and 11. We thank B.T. Draine, J. Gao, B.W. Jiang, S. Kwok and N. Meyer-Vernet for their helpful comments and suggestions. We also thank A.N. Witt and U.P. Vijn for providing us the ERE data of NGC 7023, F. Banhart and T.J. Bernatowicz, respectively, for providing us the TEM images of presolar nanodiamonds and presolar graphite with TiC nanocrystals embedded. A.L. is supported in part by a NSF grant (AST-1109039) and a NASA Herschel Theory program.

References

- Allamandola, L.J., Tielens, A.G.G.M., and Barker, J.R.: 1985, *Astrophys. J.* **290**, L25.
 Andriesse, C.D.: 1978, *Astron. Astroph.* **66**, 169.
 Andriesse, C.D. and de Vries, J.S.: 1976, *Astron. Astroph.* **46**, 143.

- Arendt, R.G., Odegard, N., Weiland, J.L., Sodroski, T.J., Hauser, M.G., Dwek, E., Kelsall, T., Moseley, S.H., Silverberg, R.F., Leisawitz, D., Mitchell, K., Reach, W.T., and Wright, E.L.: 1998, *Astrophys. J.* **508**, 74.
- Bakes, E.L.O. and Tielens, A.G.G.M.: 1994, *Astrophys. J.* **427**, 822.
- Banhart, F., Lyutovich, Y., Braatz, A., Jager, C., Henning, T., Dorschner, J., and Ott, U.: 1998, *Meteoritics and Planetary Science Supplement* **33**, 12.
- Berné, O., Joblin, C., Rapacioli, M., Thomas, J., Cuillandre, J.-C., and Deville, Y.: 2008, *Astron. Astroph.* **479**, L41.
- Bernatowicz, T.J., Amari, S., Zinner, E.K., and Lewis, R.S.: 1991, *Astrophys. J.* **373**, L73.
- Boulanger, F. and Perault, M.: 1988, *Astrophys. J.* **330**, 964.
- Bradley, J., Dai, Z.R., Erni, R., Browning, N., Graham, G., Weber, P., Smith, J., Hutcheon, I., Ishii, H., Bajt, S., Floss, C., Stadermann, F., and Sandford, S.: 2005, *Science* **307**, 244.
- Cardelli, J.A., Clayton, G.C., and Mathis, J.S.: 1989, *Astrophys. J.* **345**, 245.
- Casassus, S., Cabrera, G.F., Förster, F., Pearson, T.J., Readhead, A.C.S., and Dickinson, C.: 2006, *Astrophys. J.* **639**, 951.
- Cecchi-Pestellini, C., Mallocci, G., Mulas, G., Joblin, C., and Williams, D.A.: 2008, *Astron. Astroph.* **486**, L25.
- Chang, H.-C., Chen, K., and Kwok, S.: 2006, *Astrophys. J.* **639**, L63.
- Darbon, S., Perrin, J.-M., and Sivan, J.-P.: 1999, *Astron. Astroph.* **348**, 990.
- Desert, F.-X., Boulanger, F., and Puget, J.L.: 1990, *Astron. Astroph.* **237**, 215.
- Draine, B.T.: 2006, *Astrophysics in the Far Ultraviolet: Five Years of Discovery with FUSE* **348**, 58.
- Draine, B.T.: 2003, *Annual Review of Astronomy and Astrophysics* **41**, 241.
- Draine, B.T.: 1999, *3K Cosmology* **476**, 283.
- Draine, B.T. and Anderson, N.: 1985, *Astrophys. J.* **292**, 494.
- Draine, B.T. and Lazarian, A.: 1999, *Astrophys. J.* **512**, 740.
- Draine, B.T. and Lazarian, A.: 1998, *Astrophys. J.* **494**, L19.
- Draine, B.T. and Lee, H.M.: 1984, *Astrophys. J.* **285**, 89.
- Draine, B.T. and Li, A.: 2007, *Astrophys. J.* **657**, 810.
- Draine, B.T. and Li, A.: 2001, *Astrophys. J.* **551**, 807.
- Duley, W.W. and Seahra, S.: 1998, *Astrophys. J.* **507**, 874.
- Dwek, E., Arendt, R.G., Fixsen, D.J., Sodroski, T.J., Odegard, N., Weiland, J.L., Reach, W.T., Hauser, M.G., Kelsall, T., Moseley, S.H., Silverberg, R.F., Shafer, R.A., Ballester, J., Bazell, D., and Isaacman, R.: 1997, *Astrophys. J.* **475**, 565.
- Finkbeiner, D.P., Davis, M., and Schlegel, D.J.: 1999, *Astrophys. J.* **524**, 867.
- Godard, M. and Dartois, E.: 2010, *Astron. Astroph.* **519**, A39.
- Gordon, K.D., Witt, A.N., and Friedmann, B.C.: 1998, *Astrophys. J.* **498**, 522.
- Greenberg, J.M.: 1968, *Nebulae and Interstellar Matter*, 221.
- Habart, E., Verstraete, L., Boulanger, F., Pineau des Forêts, G., Le Peintre, F., and Bernard, J.P.: 2001, *Astron. Astroph.* **373**, 702.
- Habbal, S.R., Arndt, M.B., Nayfeh, M.H., Arnaud, J., Johnson, J., Hegwer, S., Woo, R., Ene, A., and Habbal, F.: 2003, *Astrophys. J.* **592**, L87.
- Hoang, T., Draine, B.T., and Lazarian, A.: 2010, *Astrophys. J.* **715**, 1462.
- Joblin, C., Leger, A., and Martin, P.: 1992, *Astrophys. J.* **393**, L79.
- Kapteyn, J.C.: 1904, *The Astronomical Journal* **24**, 115.
- Kharchenko, V and Lewkow, N.: 2012, Charge-Exchange and X-ray Processes with Nanodust Particles, In: Mann, I., Meyer-Vernet, N., Czechowski, A., (eds.) *Nanodust in the Solar System: Discoveries and Interpretations*, 194.
- Kimura, Y.: 2012, Phenomena of Nanoparticles in Relation to the Solar System. In: Mann, I., Meyer-Vernet, N., Czechowski, A., (eds.) *Nanodust in the Solar System: Discoveries and Interpretations*, 46.
- Ledoux, G., Ehbrecht, M., Guillois, O., Huisken, F., Kohn, B., Laguna, M.A., Nenner, I., Paillard, V., Papoular, R., Porterat, D., and Reynaud, C.: 1998, *Astron. Astroph.* **333**, L39.

- Leger, A. and Puget, J.L.: 1984, *Astron. Astroph.* **137**, L5.
- Leinert, C., Bowyer, S., Haikala, L.K., Hanner, M.S., Hauser, M.G., Levasseur-Regourd, A.-C., Mann, I., Mattila, K., Reach, W.T., Schlosser, W., Staude, H.J., Toller, G.N., Weiland, J.L., Weinberg, J.L., and Witt, A.N.: 1998, *Astronomy and Astrophysics Supplement Series* **127**, 1.
- Lewis, R.S., Ming, T., Wacker, J.F., Anders, E., and Steel, E.: 1987, *Nature* **326**, 160.
- Li, A.: 2004, *Astrophysics of Dust* **309**, 417.
- Li, A. In: Mann, I., Nakamura, A.M., and Mukai, T.: 2009, *Lecture Notes in Physics, Berlin Springer Verlag* **758**.
- Li, A. and Draine, B.T.: 2002, *Astrophys. J.* **564**, 803.
- Li, A. and Draine, B.T.: 2001, *Astrophys. J.* **554**, 778.
- Li, A. and Draine, B.T.: 2001, *Astrophys. J.* **550**, L213.
- Lodders, K.: 2005, *Chemie der Erde / Geochemistry* **65**, 93.
- Mann, I.: 2010, *Annual Review of Astronomy and Astrophysics* **48**, 173.
- Mann, I. and Czechowski, A.: 2012, Causes and Consequences of the Existence of Nanodust in Interplanetary Space, In: Mann, I., Meyer-Vernet, N., Czechowski, A., (eds.) *Nanodust in the Solar System: Discoveries and Interpretations*, 219.
- Mann, I. and Murad, E.: 2005, *Astrophys. J.* **624**, L125.
- Mann, I., Murad, E., and Czechowski, A.: 2007, *Planetary and Space Science* **55**, 1000.
- Mathis, J.S., Mezger, P.G., and Panagia, N.: 1983, *Astron. Astroph.* **128**, 212.
- Mathis, J.S., Rumpl, W., and Nordsieck, K.H.: 1977, *Astrophys. J.* **217**, 425.
- Mattila, K., Lemke, D., Haikala, L.K., Laureijs, R.J., Leger, A., Lehtinen, K., Leinert, C., and Mezger, P.G.: 1996, *Astron. Astroph.* **315**, L353.
- Onaka, T., Yamamura, I., Tanabe, T., Roellig, T.L., and Yuen, L.: 1996, *Publications of the Astronomical Society of Japan* **48**, L59.
- Ott, U.: 2007, *Space Science Reviews* **130**, 87.
- Pitz, E., Leinert, C., Schulz, A., and Link, H.: 1979, *Astron. Astroph.* **74**, 15.
- Platt, J.R.: 1956, *Astrophys. J.* **123**, 486.
- Purcell, E.M.: 1969, *Astrophys. J.* **158**, 433.
- Seahra, S.S. and Duley, W.W.: 1999, *Astrophys. J.* **520**, 719.
- Sellgren, K.: 1984, *Astrophys. J.* **277**, 623.
- Sellgren, K., Werner, M.W., and Dinerstein, H.L.: 1983, *Astrophys. J.* **271**, L13.
- Smith, T.L. and Witt, A.N.: 2002, *Astrophys. J.* **565**, 304.
- Stecher, T.P.: 1965, *Astrophys. J.* **142**, 1683.
- Steglich, M., Jäger, C., Rouillé, G., Huysken, F., Mutschke, H., and Henning, T.: 2010, *Astrophys. J.* **712**, L16.
- Szomoru, A. and Guhathakurta, P.: 1998, *Astrophys. J.* **494**, L93.
- Tanaka, M., Matsumoto, T., Murakami, H., Kawada, M., Noda, M., and Matsuura, S.: 1996, *Publications of the Astronomical Society of Japan* **48**, L53.
- Tielens, A.G.G.M.: 2008, *Annual Review of Astronomy and Astrophysics* **46**, 289.
- Trumpler, R.J.: 1930, *Publications of the Astronomical Society of the Pacific* **42**, 214.
- Vidal, M., Casassus, S., Dickinson, C., Witt, A.N., Castellanos, P., Davies, R.D., Davis, R.J., Cabrera, G., Cleary, K., Allison, J.R., Bond, J.R., Bronfman, L., Bustos, R., Jones, M.E., Paladini, R., Pearson, T.J., Readhead, A.C.S., Reeves, R., Sievers, J.L., and Taylor, A.C.: 2011, *Monthly Notices of the Royal Astronomical Society* **414**, 2424.
- Wada, S., Mizutani, Y., Narisawa, T., and Tokunaga, A.T.: 2009, *Astrophys. J.* **690**, 111.
- Watson, W.D.: 1972, *Astrophys. J.* **176**, 103.
- Weiland, J.L., Blitz, L., Dwek, E., Hauser, M.G., Magnani, L., and Rickard, L.J.: 1986, *Astrophys. J.* **306**, L101.
- Weingartner, J.C. and Draine, B.T.: 2001, *Astrophys. J.* **548**, 296.
- Weingartner, J.C. and Draine, B.T.: 2001, *The Astrophysical Journal Supplement Series* **134**, 263.
- Whittet, D.C.B.: 2003, *Dust in the galactic environment, 2nd ed. by D.C.B. Whittet. Bristol: Institute of Physics (IOP) Publishing, 2003 Series in Astronomy and Astrophysics, ISBN 0750306246.*

- Witt, A.N. and Vihj, U.P.: 2004, *Astrophysics of Dust* **309**, 115.
- Witt, A.N., Gordon, K.D., and Furton, D.G.: 1998, *Astrophys. J.* **501**, L111.
- Xiang, F.Y., Li, A., and Zhong, J.X.: 2011, *Astrophys. J.* **733**, 91.
- Ysard, N., Miville-Deschênes, M.A., and Verstraete, L.: 2010, *Astron. Astroph.* **509**, L1.

Nanodust in the Solar System: Discoveries and Interpretations

Mann, I.; Meyer-Vernet, N.; Czechowski, A. (Eds.)

2012, X, 222 p., Hardcover

ISBN: 978-3-642-27542-5